Zinc excess increases cellular demand for iron and decreases tolerance to copper in *Escherichia coli*

Received for publication, July 3, 2019, and in revised form, September 25, 2019 Published, Papers in Press, October 4, 2019, DOI 10.1074/jbc.RA119.010023

Zeling Xu[‡], Pengchao Wang[‡], Haibo Wang[§], Zuo Hang Yu[§], Ho Yu Au-Yeung[§], Tasuku Hirayama[¶], Hongzhe Sun[§], and Aixin Yan[‡1]

From the [‡]School of Biological Sciences and the [§]Department of Chemistry, University of Hong Kong, Pokfulam Road, Hong Kong, China and the [¶]Laboratory of Pharmaceutical and Medicinal Chemistry, Gifu Pharmaceutical University, 1-25-4, Dairaku-nishi, Gifu, 501-1196, Japan

Edited by Chris Whitfield

Transition metals serve as an important class of micronutrients that are indispensable for bacterial physiology but are cytotoxic when they are in excess. Bacteria have developed exquisite homeostatic systems to control the uptake, storage, and efflux of each of biological metals and maintain a thermodynamically balanced metal quota. However, whether the pathways that control the homeostasis of different biological metals cross-talk and render cross-resistance or sensitivity in the host-pathogen interface remains largely unknown. Here, we report that zinc (Zn) excess perturbs iron (Fe) and copper (Cu) homeostasis in *Escherichia coli*, resulting in increased Fe and decreased Cu levels in the cell. Gene expression analysis revealed that Zn excess transiently up-regulates Fe-uptake genes and down-regulates Fe-storage genes and thereby increases the cellular Fe quota. *In vitro* and *in vivo* protein-DNA binding assays revealed that the elevated intracellular Fe poisons the primary Cu detoxification transcription regulator CueR, resulting in dysregulation of its target genes *copA* and *cueO* and activation of the secondary Cu detoxification system CusSR-*cusCFBA*. Supplementation with the Fe chelator 2,2′-dipyridyl (DIP) or with the reducing agent GSH abolished the induction of *cusCFBA* during Zn excess. Consistent with the importance of this metal homeostatic network in cell physiology, combined metal treatment, including simultaneously overloading cells with both Zn (0.25 mM) and Cu (0.25 mM) and sequestering Fe with DIP (50 μM), substantially inhibited *E. coli* growth. These results advance our understanding of bacterial metallobiology and may inform the development of metal-based antimicrobial regimens to manage infectious diseases.

Transition metal ions are indispensable for bacterial physiology due to the key roles they play in multiple biological processes, such as protein structure stabilization, enzyme catalysis, signal transduction, etc. (1). However, excessive metals are cytotoxic due to mismetallation of enzyme active sites, thiol damage, redox stress, etc. (2–5). Thus, intracellular levels of transition metals in bacteria must be tightly regulated within a narrow range to ensure optimal growth and survival (6).

Owing to both the essentiality and cytotoxicity of transition metals to bacterial pathogens, human and other mammalian hosts have developed metal-based defending strategies against bacterial invaders by both limiting (nutritional immunity) and overloading selective transition metals at the host-pathogen interface (7, 8). For instance, iron (Fe) is the most abundant transition metal in bacteria and plays essential roles in multiple physiological processes, such as DNA replication, transcription, and central metabolism (1). Restriction of Fe availability by the production of Fe-chelating proteins, such as lactoferrin, is a common strategy of host innate immune defense against bacterial infections (9). On the other hand, copper (Cu) is a trace element important for aerobic respiration and is estimated to exist only at attomolar range in the cytosol of bacteria (10). Instead of sequestration, host macrophages overload Cu within phagolysosomes to defend *Mycobacterium tuberculosis* infections (11, 12). Zinc (Zn) is the second most abundant transition metal in bacteria with functional importance in enzyme catalysis and protein structures. In the mammalian host, Zn concentrations are reported to range from 5 μM in the nasopharynx to ~300 μM in the lung tissues (13). Both Zn sequestration by the calprotectin protein and Zn poisoning in phagolysosomes (up to 0.46 mM Zn) have been reported to be employed by the host to combat bacterial infections (14–17).

On the other hand, bacteria have evolved sophisticated metal homeostatic systems as their virulence factors to compete for the metals in deficiency or expel those in excess to maintain optimal cellular metal contents for their physiology and survival (18). Although homeostatic pathways for each of the individual biological metals are relatively well-understood (10), whether the different metal homeostatic pathways cross-talk and render cross-resistance or sensitivity at the host-pathogen interface remains largely elusive. Several previous studies reported that excessive Zn interferes the metallation of various non-Zn metalloenzymes and proteins. For instance, in *Streptococcus pneumoniae*, Zn was demonstrated to bind pneumococcal surface adhesin A (PsaA) and block Mn uptake (19). In *Bacillus subtilis*, Zn was reported to cause dysregulation of the PerR regulon and cause heme toxicity (20). In the Gram-negative bacterium *Escherichia coli*, Zn was shown to cause mismet-

This study was supported by Seed Funding for Strategic Interdisciplinary Research Scheme HKU 2017 (to A. Y.) and Health and Medical Research Fund (HMRF) Grant 18171042 (to A. Y.). The authors declare that they have no conflicts of interest with the contents of this article.

This article contains Tables S1 and S2 and Figs. S1–S7.

[1] To whom correspondence should be addressed: School of Biological Sciences, University of Hong Kong, Pokfulam Road, Hong Kong, China. Tel.: 852-22990864; Fax: 852-25599114; E-mail: ayan8@hku.hk.

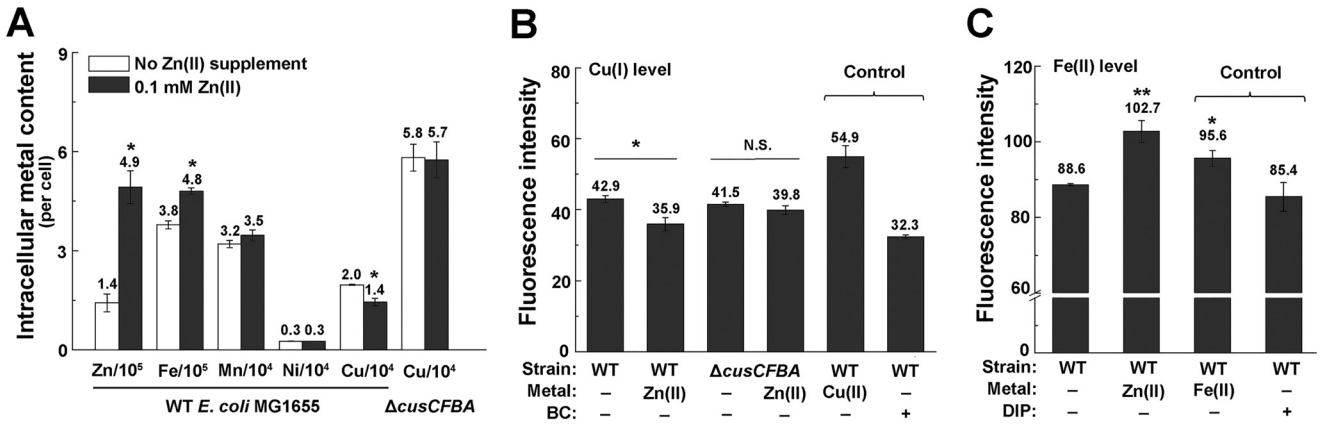

Figure 1. Zn excess leads to alteration of intracellular Cu and Fe contents. *A*, intracellular content of physiologically relevant metals in *E. coli* MG1655 cells in the absence and presence of excessive Zn (0.1 mM). *B*, intracellular Cu(I) content measured using the Cu(I) probe N4HMF in the indicated strains and conditions. 0.5 μM bathocuproine (BC) was used. *C*, intracellular Fe(II) content measured using the Fe(II) probe HMRhoNox-M. 50 μM 2, 2′-dipyridyl (DIP) was used. *Error bars*, S.D. *, $p < 0.05$; **, $p < 0.01$ *versus* no metal treatment (based on Student's *t* test).

allation of mononuclear iron enzymes and damage [Fe-S] cluster–containing dehydratases, resulting in metabolic arrest and cell death (21). However, a systematic investigation of the interplay of Zn homeostasis with the homeostasis of other physiological transition metals is lacking.

In the present study, we undertake to investigate this physiological process and show that Zn excess perturbs the Fe and Cu homeostasis in *E. coli*, resulting in an increased demand for Fe supply and a decreased tolerance to Cu toxicity. These findings demonstrated the complexity of metallobiology at the host-pathogen interface and provided implications for the development of metal-based antimicrobial treatment.

Results

Zn excess leads to alteration of intracellular Cu and Fe contents in E. coli

To investigate whether Zn stress perturbs the homeostasis of other transition metals in *E. coli*, we set out to measure intracellular contents of the physiologically relevant transition metals Zn, Fe, Cu, Mn, and nickel (Ni) in *E. coli* MG1655 cells cultured to OD_{600}[2] of 0.4 under Zn stress. Because macrophages infected with *M. tuberculosis* were reported to overload up to 0.46 mM Zn to combat the pathogen (14), and previous studies applied 0.1–0.5 mM Zn to generate moderate to severe Zn stress in various bacterial species (5, 20, 22–24), we first chose 0.1 mM Zn, which elicits a moderate Zn stress but did not significantly inhibit the growth of *E. coli* in our investigations. Inductively coupled plasma-mass spectrometry (ICP-MS) analysis showed that in addition to an obvious elevation of Zn content in these cells, a decreased Cu content and an increased Fe content was observed (Fig. 1*A*), whereas the contents of Mn and Ni remained unchanged. These results suggested that Zn stress perturbed Cu and Fe homeostasis in *E. coli* cells. To verify the altered Cu and Fe content in *E. coli* cells under Zn stress, we used fluorescent Cu(I) probe N4HMF (25) and Fe(II) probe HMRhoNox-M (26) to detect the intracellular labile Cu(I) and Fe(II) contents, respectively. Consistent with the ICP-MS result, a decreased intracellular Cu(I) content and an increased Fe(II) content were observed in *E. coli* cells cultured under Zn stress (0.1 mM) compared with that without Zn excess (Fig. 1, *B* and *C*), confirming that Zn excess altered Cu and Fe homeostasis in *E. coli*.

The Cu efflux operon cusCFBA is induced during Zn excess by the Cus system regulator CusRS

Because a previous microarray analysis by Lee *et al.* showed that Cu/silver (Ag) efflux genes *cusCFBA* (Fig. 2*A*) were up-regulated during Zn excess in *E. coli* (27), we next examined whether the decreased Cu content observed during Zn excess was caused by overproduction of the CusCFBA efflux pump. β-gal activity assay of the P_{cusC}-*lacZ* transcription fusion showed that transcription of the *cusCFBA* operon was indeed significantly induced in the presence of 0.1 or 0.2 mM Zn (Fig. 2*B*), and the induction was continuous and achieved the maximal level in the late exponential phase (Fig. S1, *A* and *B*). Measuring the RNA level of *cusC* and the production of chromosomal CusC-FLAG confirmed the significant induction of the efflux system during Zn excess (Fig. 2*C* and Fig. S1*C*). Deletion of the *cusCFBA* operon led to an elevation of Cu content in *E. coli* cells both with and without excess Zn, but applying Zn stress no longer led to the decrease of Cu content in this strain background (Fig. 1, *A* and *B*). These results indicated that the reduced intracellular Cu content during Zn excess was caused by the overproduction of the Cu efflux system CusCFBA.

Expression of the *cusCFBA* operon is known to be regulated by the Cus (Cu-sensing locus) system regulator, the two-component system CusRS (Fig. 2*A*) (28, 29). To investigate whether induction of the *cusCFBA* operon during Zn excess was dependent on CusRS, we deleted *cusRS* and found that transcription of P_{cusC}-*lacZ* and production of the chromosomal CusC-FLAG was completely abolished in the mutant during Zn excess (Fig. 2, *B* and *C*), demonstrating that up-regulation of the Cu efflux system *cusCFBA* during Zn excess was dependent on CusRS, which senses Cu(I) species (30). To investigate the Cu(I) sources

[2] The abbreviations used are: OD, optical density; BC, bathocuproine; BCS, bathocuproine disulfonate; DIP, 2, 2′-dipyridyl; EMSA, electrophoretic mobility shift assay; ICP-MS, inductively coupled plasma-mass spectrometry; qPCR, quantitative PCR; CouA, L-(7-hydroxycoumarin-4-yl) ethylglycine; ppb, parts per billion; LB, lysogeny broth; ROS, reactive oxygen species; FRET, förster resonance energy transfer.

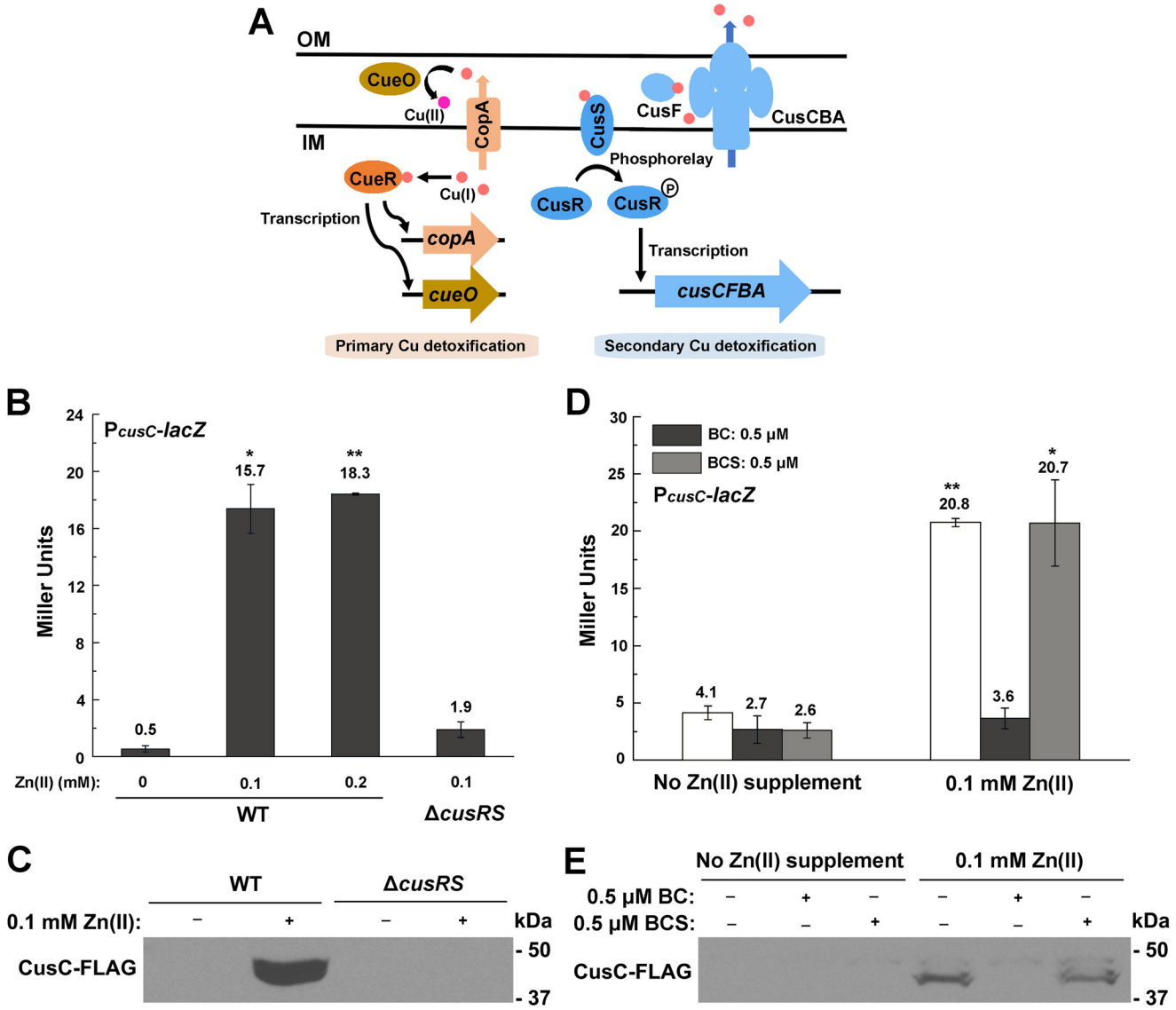

Figure 2. *cusCFBA* system is induced by intracellular Cu in a CusRS-dependent manner during Zn excess. *A*, *schematic diagram* of the primary and secondary Cu homeostatic systems in *E. coli*. *OM*, outer membrane; *IM*, inner membrane. *B* and *D*, β-gal activities of P_{cusC}-*lacZ* transcriptional fusion during Zn excess in WT *E. coli* cells and Δ*cusRS* mutant (*B*) and in the presence of Cu chelators BC and BCS, respectively (*D*). *C* and *E*, production of chromosomal CusC-FLAG in WT and Δ*cusRS* mutant during Zn excess (C) and that in the presence of Cu chelators (*E*). *Error bars*, S.D. *, $p < 0.05$; **, $p < 0.01$ *versus* no Zn treatment (based on Student's *t* test).

that activated CusRS, we supplemented membrane-permeable Cu(I)-specific chelator bathocuproine (BC) or membrane-impermeable Cu(I) chelator bathocuproine disulfonate (BCS) (31) and examined their effect on the expression of *cusCFBA* during Zn stress. We found that while BC completely abolished the transcription of P_{cusC}-*lacZ* and production of chromosomal CusC-FLAG during Zn stress, BCS had no effect on *cusC* expression under this condition (Fig. 2, *D* and *E*), demonstrating that the endogenously originated Cu(I) induced the up-regulation of *cusCFBA*. Together, these results confirmed that reduction of Cu content during Zn excess was due to the activation of the Cu efflux system CusCFBA by the Cus system regulator CusSR.

Zn excess leads to inactivation of the primary Cu detoxification system

CusCFBA is known to be capable of exporting both Cu(I) and Ag(I) ions upon induction. To further confirm the induction of the CusCFBA and examine its physiological effect during Zn excess, we pretreated *E. coli* cells with Zn stress (0.1 mM) and subjected the cells to Cu and Ag sensitivity assay. Consistent with the overproduction of the CusCFBA efflux pump during Zn treatment, *E. coli* cells pretreated with Zn displayed higher tolerance to Ag(I) than the untreated cells (Fig. 3*A*). Unexpectedly, these cells displayed reduced Cu tolerance compared with the untreated cells (Fig. 3*A*). Similar results were also observed in a clinical isolate of uropathogenic *E. coli* UTI-1 (Fig. 3*A*).

These results implied the presence of Cu detoxification defects in *E. coli* cells challenged with Zn stress that could not be compensated by the induction of CusCFBA. In addition to the CusCFBA efflux system, it is known that *E. coli* contains the primary detoxification system Cue, which includes the Cu-translocating P-type ATPase CopA and the periplasmic multicopper oxidase CueO under the control of the transcriptional regulator CueR (Fig. 2*A*) (32, 33). CopA functions to export

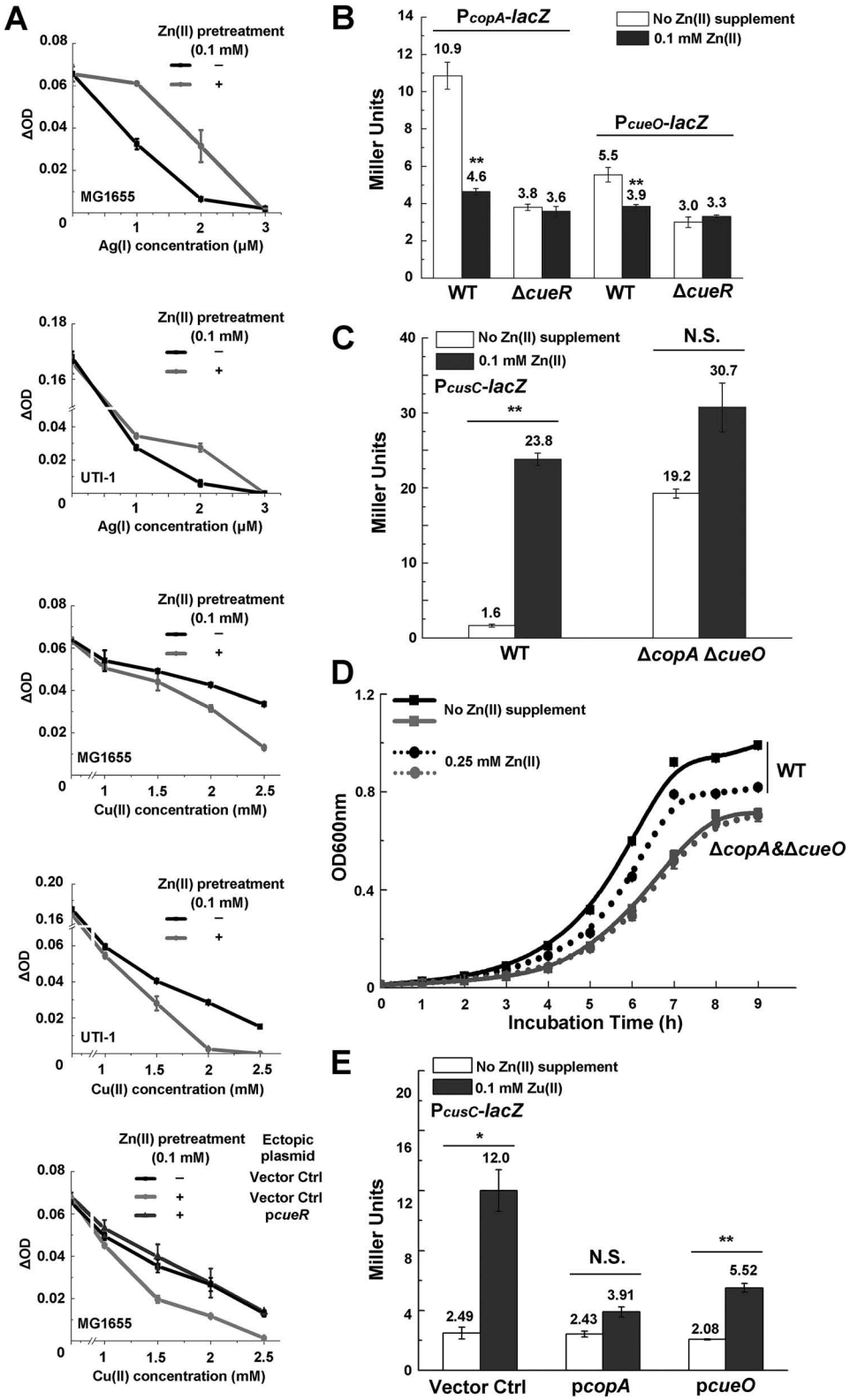

Figure 3. Zn excess led to defect of the primary Cu detoxification system Cue. *A*, Ag and Cu sensitivity of WT *E. coli* MG1655, clinical UTI-1, and MG1655 strains with the pET28a vector (*Vector Ctrl*) or pET28a-*cueR* (P_{cueR}) in the presence or absence of 0.1 mM Zn pretreatment. OD increase of different strains is measured after growth for 2 h in various concentrations of Cu(II). *B*, β-gal activities of P_{copA}-*lacZ* and P_{cueO}-*lacZ* transcriptional fusions during Zn excess in *E. coli* WT and Δ*cueR* mutant. *C*, β-gal activities of P_{cusC}-*lacZ* transcriptional fusion during Zn excess in *E. coli* WT and Δ*copA*Δ*cueO* mutant. *D*, growth of *E. coli* WT and Δ*copA*Δ*cueO* mutant in the presence or absence of 0.25 mM Zn. *E*, β-gal activities of P_{cusC}-*lacZ* transcriptional fusion during Zn excess in WT *E. coli* MG1655 strains with the pET11a vector (*Vector Ctrl*), pET11a-*copA* (P_{copA}), or pET11a-*cueO* (P_{cueO}). *Error bars*, S.D. *N.S.*, not significant; *, $p < 0.05$; **, $p < 0.01$ *versus* no Zn treatment (based on Student's *t* test).

cytoplasmic Cu(I) to the periplasmic space, and CueO oxidizes Cu(I) to the less toxic Cu(II) species (34–36). We then measured the expression levels of both *cueO* and *copA* genes under Zn stress by β-gal activity assays (Fig. 3*B*) and RT-quantitative PCR (qPCR) (Fig. S2), and found that expression of both genes was significantly reduced under this condition, verifying the defect of the primary Cu detoxification system during Zn stress. Transcription of the *cusCFBA* operon during Zn excess was found to be similar to that in the Δ*copA* Δ*cueO* double deletion *E. coli* cells without Zn excess (Fig. 3*C*), suggesting that the induction of the CusCFBA during Zn stress was likely due to the interference of Cu homeostasis caused by inactivation of both *copA* and Δ*cueO*. Consistent with this notion, in the Δ*copA* Δ*cueO* cells, Zn stress no longer led to significant induction of the *cusCFBA* operon (Fig. 3*D*), and the cells became insensitive to Zn challenge, as reflected by the unaltered growth curve of the cells with or without Zn stress (0.25 mM) (Fig. 3*D*). Moreover, ectopic overexpression of *copA* or *cueO* significantly abolished the induction of the *cusCFBA* operon during Zn excess (Fig. 3*E*) and partially restored the Cu tolerance of *E. coli* cells pretreated with excessive Zn (Fig. S3). Together, these results indicated that Zn stress caused damage of the primary Cu detoxification system CopA and CueO, resulting in a defect of Cu homeostasis in *E. coli* cells, which triggered the induction of the secondary Cu detoxification system CusCFBA.

Because expression of *copA* and *cueO* is regulated by the transcription regulator CueR in *E. coli* (Fig. 2*A*) (32), we next investigated whether expression defect of *copA* and *cueO* during Zn excess was caused by dysregulation of CueR. Indeed, in Δ*cueR* cells, Zn excess no longer caused decrease of the expression of *copA* and *cueO* (Fig. 3*B*), and ectopic overexpression of *cueR* completely restored the Cu tolerance of *E. coli* cells pretreated with 0.1 mM Zn to the level of untreated cells (Fig. 3*A*). Together, these results indicated that Zn excess led to dysregulation of CueR and the defect of Cu detoxification, which was not fully compensated by the induction of CusCFBA.

Perturbation of Cu homeostasis during Zn excess is mediated by intracellular Fe accumulation

Next, we sought to identify the molecular mechanism of CueR dysregulation during Zn excess. One possibility is that Zn may cause mismetallation of CueR and inhibit its activation of the target *copA* and *cueO* promoters. To test this, we performed electrophoretic mobility shift assay (EMSA) to examine whether Zn abolishes the binding of CueR to the *copA* and *cueO* promoter DNA. However, we found that supplement of Zn (0.2 mM) did not lead to dissociation of CueR from the two promoters (Fig. 4*A*). Interestingly, when we supplemented Fe (0.2 mM), the content of which was increased in *E. coli* cells during Zn excess (Fig. 1, *A* and *C*), we observed that the oxidized form Fe(III), but not the reduced form Fe(II), led to dissociation of CueR from the CueR-P_{copA} and CueR-P_{cueO} complexes (Fig. 4*A*). This result suggested that CueR dysregulation might be caused by the elevated Fe under this condition. To investigate this process *in vivo*, we examined the interaction of CueR with its target promoters using a FRET-based *in vivo* protein-DNA binding assay developed by us[3] (Fig. 4*B*). Structural studies have demonstrated that CueR binds to its target *copA* and *cueO* promoters as a repressor in the absence of the inducing signal Cu and as an activator in the presence of Cu (37). During the transcription activation, Cu binding triggers an allosteric switch of the protein-DNA complex, allowing the DNA-binding domains of the CueR dimer to tightly clamp into the DNA major grooves and introducing a substantial (22°) DNA undertwist that favors RNA polymerase recognition (37). To monitor this conformational change *in vivo* and examine the effect of various metal stresses on the regulation process, we inserted a fluorescent unnatural amino acid L-(7-hydroxycoumarin-4-yl) ethylglycine (CouA) at the loop region between the α3 and α4 of the DNA-binding domain of CueR using the genetic codon expansion approach (38) and utilized SYTO9 to label DNA. An increased FRET efficiency between the CouA donor in CueR to the SYTO9 acceptor bound to the promoter DNA will indicate the bending of DNA and subsequent activation of these promoters by CueR (Fig. 4*B*). As shown in Fig. 4 (*C* and *D*), compared with the signal in the absence of Cu, an obvious FRET effect with a calculated efficiency of 38.9% was observed between CouA and SYTO9 upon the addition of 0.1 mM Cu. Interestingly, adding 0.1 mM Zn abolished this FRET effect to the level of no metal signal (efficiency 36.3%). Further supplementing the Fe(II) chelator 2, 2′-dipyridyl (DIP) (39) restored the FRET efficiency (efficiency 37.6%). This result confirmed that activation of its target *copA* and *cueO* promoters by CueR was indeed disrupted by elevated Fe during Zn stress.

Consistent with this notion, supplementing DIP reversed the expression changes of *copA*, *cueO*, and *cusC* in *E. coli* cells caused by Zn stress and restored their expression to their native levels without Zn stress (Fig. 4*E*). Furthermore, Cu tolerance in *E. coli* MG1655 and UTI-1 cells pretreated with Zn was also restored by supplementation of DIP (Fig. 4*F*). These results demonstrated that perturbation of Cu homeostasis by Zn excess, including the down-regulation of *cue* regulon and up-regulation of *cus*, was mediated by intracellular accumulation of Fe under this condition.

Increased Fe uptake and oxidative stress are responsible for the perturbation of Cu homeostasis during Zn excess

In vitro EMSA suggested that Fe(III), but not Fe(II), interfered with the binding of CueR to *copA* and *cueO* promoters (Fig. 4*A*). It is well-known that Fe accumulation can lead to oxidative stress by Fenton reaction ($H_2O_2 + Fe^{2+} \rightarrow Fe^{3+} + HO^{\bullet} + OH^-$) (40). To explore whether Zn excess led to increased oxidative stress in the cell, we first detected the intracellular ROS level using the probe CM-H_2DCFDA (41) and found that intracellular ROS levels increased with increasing concentration of Zn treatment (Fig. 5*A*). To investigate whether oxidative stress indeed was necessary to cause CueR dysregulation during Zn excess, we cultured *E. coli* cells under anaerobic conditions and measured the transcription of *copA*, *cueO*, and *cusC* during Zn excess. Despite the fact that Fe(II) also accumulated during anaerobic Zn stress (Fig. S4), we found

[3] Z. Xu, P. Wang, H. Wang, Z. Hang Yu, H. Y. Au-Yeung, T. Hirayama, H. Sun, and A. Yan, unpublished observations.

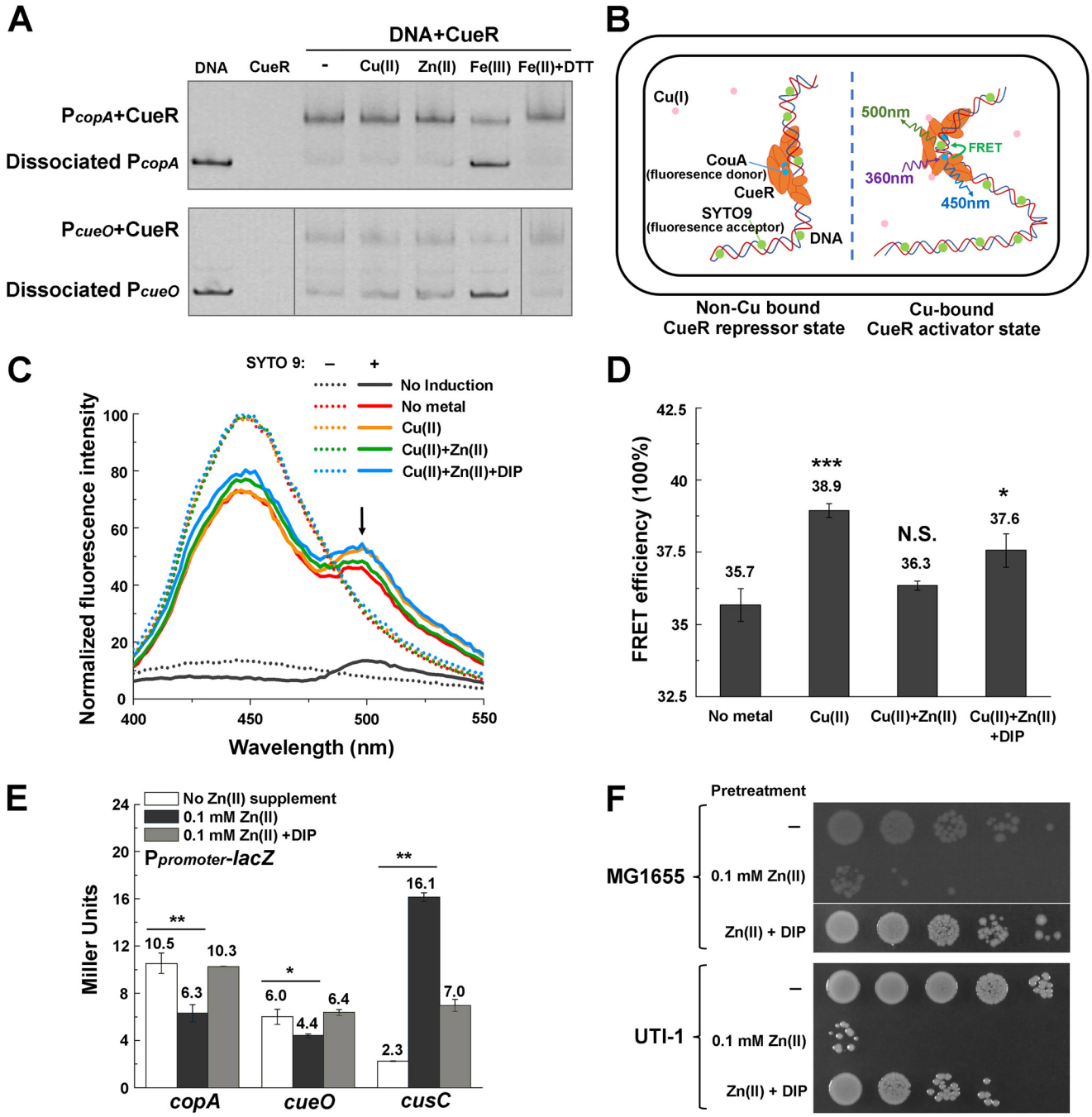

Figure 4. Perturbation of Cu homeostasis during Zn excess is mediated by intracellular accumulation of Fe. *A*, EMSA analysis of the binding of CueR to *copA* and *cueO* promoter in the presence of Cu(II), Zn(II), Fe(III), and Fe(II) with DTT, respectively. The *last lane* in the *bottom panel* is from a different gel. *B*, schematic diagram of the FRET-based *in vivo* CueR-promoter binding assay. A fluorescent unnatural amino acid donor CouA (*blue dots*; excitation 360 nm, emission 450 nm) is incorporated into CueR protein by replacing the Phe-58 residue in its DNA-binding domain. SYTO9 (green dots; excitation 483 nm, emission 503 nm) is utilized to label DNA. Upon Cu binding to CueR and an allosteric switch from the repressor state to the activator state, an efficient FRET effect between the CouA-SYTO9 pair can be recorded with excitation at 360 nm. FRET efficiency changes can be calculated to indicate the distance change required for CueR activation. *C* and *D*, emission spectra (*C*) and FRET efficiency changes (*D*) of the CouA-SYTO9 pair in the presence of 0.1 mM Cu(II), 0.1 mM Cu(II) + 0.1 mM Zn(II), or 0.1 mM Cu(II) + 0.1 mM Zn(II) + 0.2 mM DIP. *E*, β-gal activities of P_{cusC}-*lacZ*, P_{copA}-*lacZ* and P_{cueO}-*lacZ* transcriptional fusions during Zn excess with or without the supplement of 50 μM Fe(II) chelator DIP. *F*, Cu tolerance of *E. coli* MG1655 and clinical isolate UTI-1 strain subjected to Zn pretreatment or Zn pretreatment in the presence of 50 μM DIP. The *bottom row* in the *top panel* is from a different plate. *Error bars*, S.D. *, $p < 0.05$; **, $p < 0.01$; ***, $p < 0.001$ *versus* no Zn (metal) treatment (based on Student's *t* test).

that expression of these Cu homeostasis genes was not significantly altered by Zn stress (Fig. 5*B*). Furthermore, when the reductant glutathione (GSH) was supplemented during Zn stress under aerobic conditions, induction of the *cusCFBA* operon was completely abolished (Fig. 5*C*). No growth defect was observed when *E. coli* cells were challenged with an even higher concentration of Zn (0.5 mM) under anaerobic conditions (Fig. S5). These results demonstrated that both intracellular accumulation of Fe and oxidative stress led to dysregulation of CueR during Zn excess.

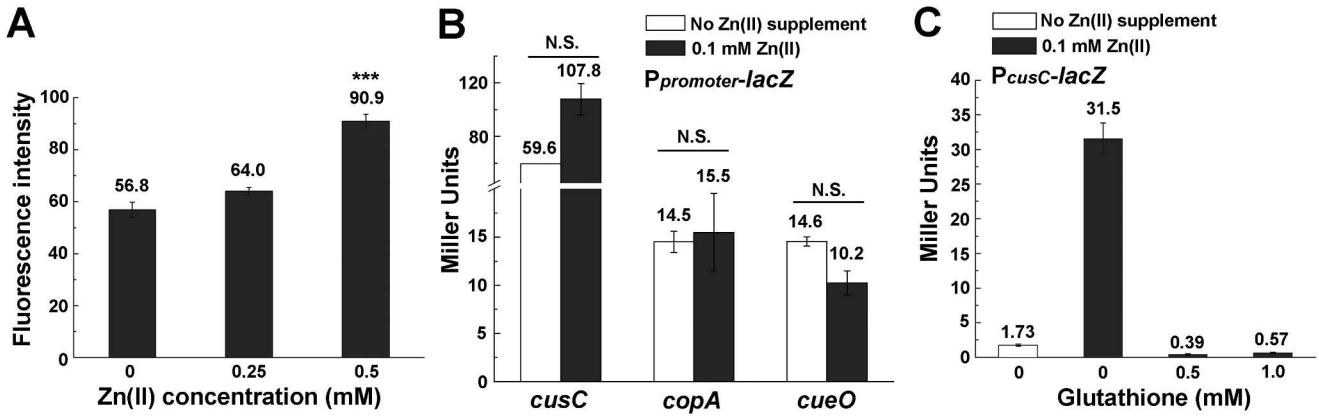

Figure 5. Oxidative stress contributes to the perturbation of Cu homeostasis during Zn excess. *A*, intracellular ROS level of *E. coli* MG1655 in the presence of excessive Zn measured using the probe CM-H_2DCFDA. *B*, β-gal activities of P_{cusC}-*lacZ*, P_{copA}-*lacZ*, and P_{cueO}-*lacZ* challenged with Zn excess under anaerobic conditions. *C*, β-gal activities of P_{cusC}-*lacZ* during Zn excess with or without the supplementation of GSH. ***, $p < 0.001$ *versus* no Zn treatment (based on Student's *t* test). *Error bars*, S.D.

Fur regulon is transiently dysregulated during the adaptation to Zn stress

We next asked how Fe content was accumulated during Zn excess. We measured Fe content of the culture medium of *E. coli* cells grown to OD_{600} of 0.4 under Zn excess (0.1 mM) conditions and found that its level (85.4 ppb) was lower than that in the culture medium of the cells grown without Zn supplement (97.2 ppb) (Fig. 6*A*), indicating that intracellular Fe accumulation was due to increased Fe uptake during Zn excess. Because Fe uptake is primarily regulated by the Fe-binding transcription regulator Fur, we then examined the expression of Fur regulon genes, including those involved in Fe uptake and Fe storage in cells grown to mid-log phase (OD_{600} of 0.4) under Zn excess conditions. Surprisingly, we observed down-regulation of Fe-uptake genes (*tonB*, *entC*, *fiu*, *feoA*, *fepA*, and *fecA*) and up-regulation of a Fe-storage gene (*ftnA*) in these cells (Fig. S6*A*). Although the data fail to explain how Fe uptake was achieved, they are consistent with the increased Fe content under this condition, which should result in the activation of the Fur regulon (*i.e.* decreased expression of Fe-uptake genes and increased expression of Fe-storage genes).

Because cells grown to OD_{600} of 0.4 represent a status that has adapted to Zn excess, we speculated that there was a transient increase of Fe uptake in the early stage of adaptation to Zn stress. To test this, we first grew *E. coli* cells to OD_{600} of 0.3 without Zn stress and then subjected the cells to Zn stress (0.1 mM). We monitored the dynamic expression of Fur regulon genes at different time points upon the switch (*i.e.* 10 min, 30 min, 1 h, and 2 h) (Fig. 6*B* and Fig. S6) and found an obvious up-regulation of Fe-uptake genes and down-regulation of Fe-storage genes at the 30-min time point (Fig. 6*B* and Fig. S6*C*), implying the dysregulation of Fur at this early adaptation stage and consequently derepression of the Fe-uptake genes and repression of the Fe-storage genes. The expression pattern was reversed after the 60-min time points (Fig. 6*B* and Fig. S6*D*) (*i.e.* Fe-uptake genes were down-regulated, and Fe-storage genes were up-regulated), reflecting the restoration of Fur activity and regulation by elevated Fe content through Fe uptake at the adaptation stage. Together, these results suggested that Zn excess led to a transient dysregulation of Fur until a new equilibrium was established with a higher Fe quota in the cell.

Enhanced Fe uptake and Cu efflux are required to adapt to Zn excess

To investigate the contribution of increased Fe uptake and Cu efflux to cell physiology of *E. coli* under Zn stress, we tested the growth of *E. coli* cells challenged with Zn excess in the standard MOPS medium with sufficient Fe or Fe-depleted MOPS medium (without adding Fe source). As shown in Fig. 7*A*, growth of *E. coli* cells in Fe-depleted medium was completely inhibited when they were challenged with Zn excess, whereas their growth in Fe-sufficient medium remained unchanged despite the Zn stress, suggesting that during Zn excess, *E. coli* cell demands a higher Fe supply to maintain its growth. We also performed a competition assay of the WT and isogenic Δ*cusC* cells following co-culturing in MOPS medium with or without 0.5 mM Zn. Competitive index, which is defined as the ratio of viable Δ*cusC* cells *versus* the viable WT cells, was utilized to indicate the fitness of the cells (42). As shown in Fig. 7*B*, whereas the Δ*cusC* cells out-competed the WT cells with a competitive index of 1.86 without Zn stress, the cells lacking *cusC* displayed a fitness disadvantage in the presence of 0.5 mM Zn with a competitive index of 0.81. This result suggested that failure of inducing the CusCFBA efflux system to export intracellular Cu(I) conferred a fitness disadvantage to *E. coli* during Zn stress.

To explore whether the adaptive cross-talk of Zn, Fe, and Cu homeostatic pathways has implications for the metal-based antimicrobial treatment, we interfered with the cross-talk by supplementing Fe chelator and excessive Cu and examined the growth of *E. coli* cells with these interferences (*i.e.* growth under Zn excess, Zn excess and Cu overloading (0.25 mM), and Zn excess combined with both Cu overloading and Fe sequestration by the chelator DIP (50 μM)). Consistent with our findings, interfering with the adaptive cross-talk of metal homeostasis by simultaneous overloading of Cu and sequestering of Fe during Zn excess (0.25 mM) significantly inhibited the growth of *E. coli* cells (Fig. 7*C*), demonstrating the potential of applying

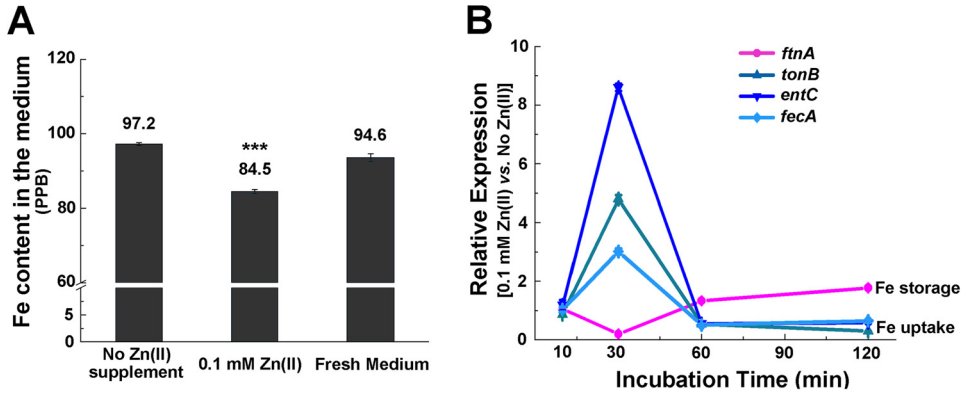

Figure 6. Fe uptake was increased by transient up-regulation of Fe-uptake genes and down-regulation of Fe-storage genes following Zn shock. *A*, ICP-MS analysis of Fe content in the spent medium of *E. coli* grown with or without Zn excess. *B*, transcripts of Fe-uptake (*fecA*, *entC*, and *tonB*) and Fe-storage (*ftnA*) genes measured at various time points following the switch to Zn excess. *Error bars*, S.D. ***, $p < 0.001$ *versus* no Zn treatment (based on Student's *t* test).

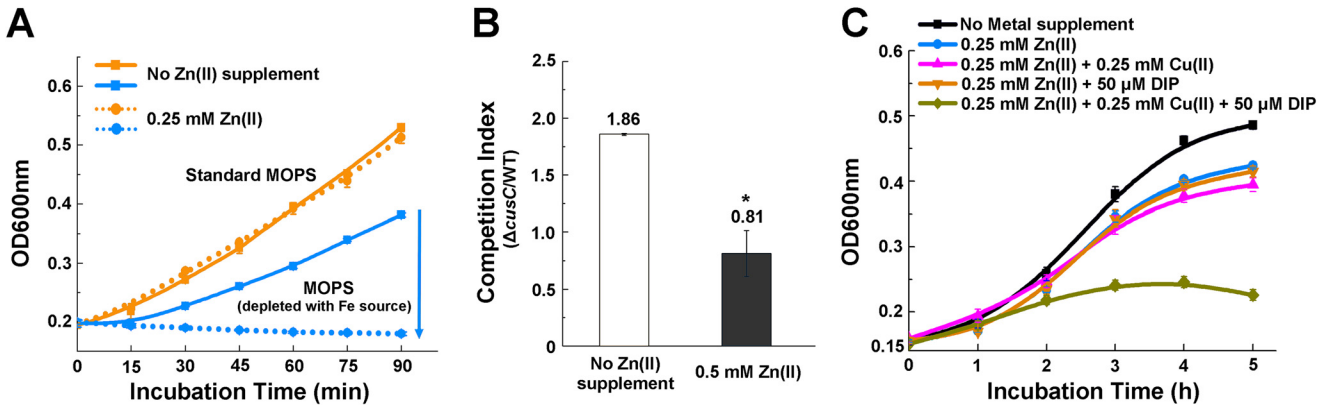

Figure 7. Fe uptake and Cu efflux are required to maintain cell fitness during Zn excess. *A*, growth of *E. coli* cells challenged with Zn excess in Fe-sufficient or -depleted MOPS medium. *B*, competition assay between the WT and Δ*cusC* mutant with or without Zn excess. *C*, growth curve of *E. coli* cells challenged with the different combinations of Zn, Cu, and Fe(II) chelator DIP. *Error bars*, S.D. *, $p < 0.05$ *versus* no Zn treatment (based on Student's *t* test).

combined metal intoxication and metal sequestration to control pathogens.

Discussion

Despite the co-occurrence of the excess and depletion of different biological metals in the various environmental settings and the host-pathogen interfaces, the interplay of the different metal homeostatic pathways and their contribution to bacterial physiology and stress adaptation remained elusive. In this study, we uncovered the adaptive cross-talk of Zn, Fe, and Cu homeostatic pathways in *E. coli* in response to Zn excess. Overloading *E. coli* cells with Zn led to transient dysregulation of the Fe homeostasis regulator Fur and consequently the derepression of Fe-uptake genes and repression of Fe-storage genes, resulting in the overloading of Fe in the cell. Elevated Fe quota combining with increased oxidative stress under this condition poisoned the primary Cu detoxification transcription regulator CueR, which caused decreased expression of the P-type Cu exporter CopA and the Cu oxidase CueO. In response to this defect, *E. coli* cells activated the secondary Cu detoxification system CusCFBA through the CusRS signaling transduction pathway to lower the intracellular Cu content (Fig. 8). Consequently, *E. coli* cells challenged with Zn excess display an increased demand for Fe and decreased tolerance to Cu. This mechanism underlies the strategies employed by the host immune system to combat bacterial infections, which often involve simultaneous overloading of Zn and Cu and deprivation of Fe (43, 44).

Despite the diversity of their cognate metal types and coordination geometry, metalloenzymes select metals imperfectly, and they display a common order of metal affinities following the Irving–Williams series (*i.e.* with a higher affinity for Cu(I) and Zn(II) than for Mn(II) and Fe(II)) (45). Metal specificity in the cell is largely maintained by the tight regulation of buffered cytoplasmic metal pools, which match the binding dissociation constants of their corresponding metal-binding transcription regulators (46–48). For instance, the relatively high labile Fe(II) pool ($\sim 10^{-4}$ M) and the relative low dissociation constant of Fur ($K_d = 10^{-6}$ M) warrants the correct metallation of Fe-containing enzymes and prevents mismetallation of the enzymes by other metals, such as Zn (46, 49). However, tighter affinity to incorrect metals is a risk for mismetallation and renders the corresponding metalloproteins vulnerable to metal toxicity (47, 50). In addition to Fe(II), several other divalent cations, including Co, Mn, Zn, and the oxidized Fe(III), have been shown to be able to bind to Fur and modulate its DNA-binding properties (49). Among them, Zn(II) displayed the highest affinity to Fur, with a K_d of $\sim 1.4 \times 10^{-10}$ M. In the nonstressed cells, mismetallation of Fur by Zn is prevented by the tightly controlled free Zn concentration ($\sim 10^{-15}$ M) (51). However, overloading of Zn may shift this thermodynamic equilibrium. Indeed, mismetal-

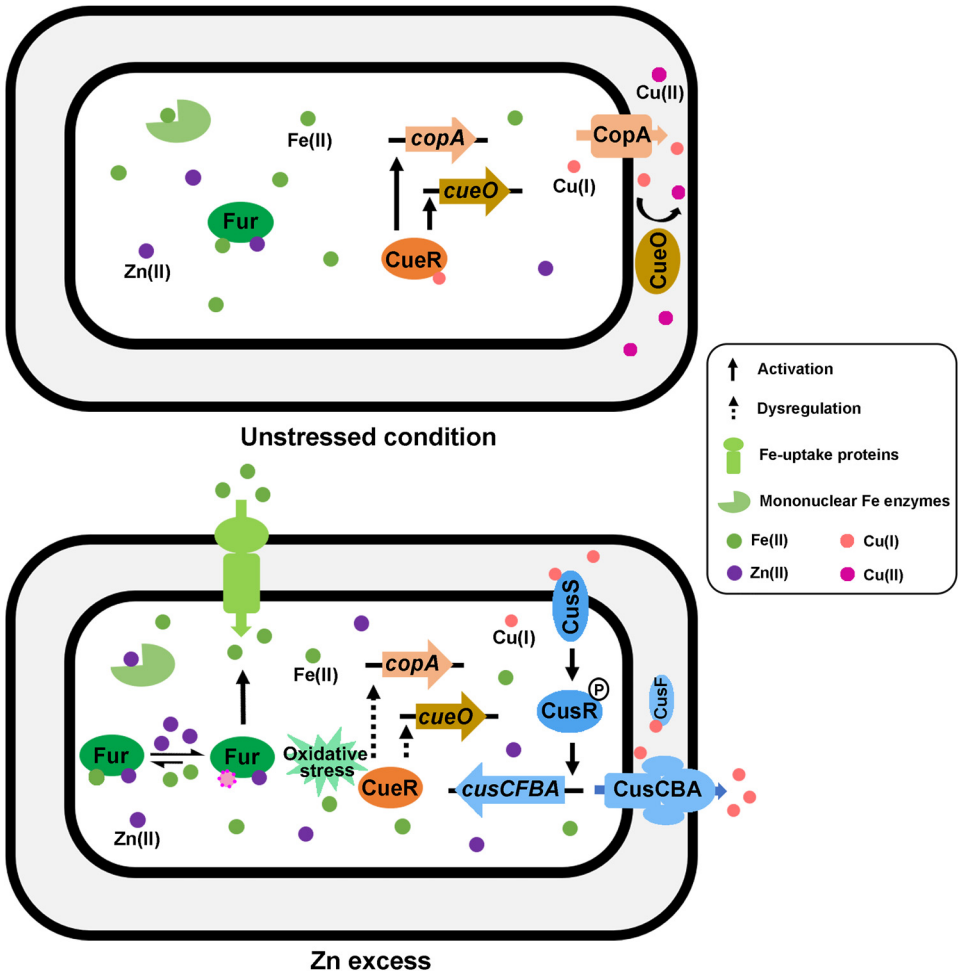

Figure 8. A working model illustrating the cross-talk of Zn, Fe, and Cu homeostatic pathways in response to Zn excess in *E. coli* MG1655. A balanced metal quota of Zn, Fe, and Cu is maintained in *E. coli* cells to ensure the correct metallation of metal-containing enzymes in *E. coli* cells (*top*). During Zn excess (*bottom*), Zn overloading shifted the equilibrium of labile Zn and Fe contents in *E. coli* cells, which caused mismetallation of mononuclear Fe-containing enzymes and a transient dysregulation of Fur. Fur dysregulation led to the up-regulation of the Fe-uptake genes, resulting in an elevation of Fe content in the cell. Elevated Fe combining with oxidative stress under this condition poisoned the primary Cu detoxification regulator CueR, which down-regulated *copA* and *cueO* and triggered the activation of the secondary Cu detoxification system CusCFBA to lower the Cu quota in the cell.

lation of solvent-exposed mononuclear Fe-containing enzymes, such as threonine dehydrogenase (Tdh), ribulose-5-phosphate 3-epimerase (Rpe), and 3-deoxy-D-arabinoheptulosonate-7-phosphate synthase (DAHPS), by excessive Zn (0.15 mM) in the *zntA*-deficient *E. coli* background has been reported (21). In this study, we also measured the Tdh activity of *E. coli* cells following the switch to Zn-excessive conditions and observed an immediate (5-min) reduction of the Tdh activity (Fig. S7). After the 30-min time point, the activity of the enzyme was recovered (Fig. S7), which was concurrent with the increased expression of Fe-uptake genes at this time point (Fig. S6). These data suggested the disruption of Fe metallation in the mononuclear Fe-containing enzymes during Zn excess. Whether a similar manner of mismetallation occurred in Fur is not known. Nonetheless, an obvious transient dysregulation of Fur was observed in the initial adaptation stage to Zn stress (Fig. 6*B*). Transient alteration of Fur and SoxS regulon in the chemostat *E. coli* culture challenged with Zn excess was also reported by Graham *et al.* (52). These results imply that Fur might be mismetallated during Zn excess, which could be caused by a surge of Zn content during Zn stress prior to the activation of the Zn homeostatic components or by the produced Fe(III) owing to elevated Fe content and oxidative stress, both of which have been shown to be able to bind to Fur (49). As a result, a new equilibrium with an increased Fe content was established to maintain the correct metallation of Fe-containing enzymes under Zn-stress conditions (Fig. 8).

Cross-talk of Fe and Cu homeostatic systems has also been described by several previous studies, but the underlying mechanisms remained largely unclear. In the yeast *Saccharomyces cerevisiae*, Fe uptake was found to be dependent on the Cu transport protein CTR1 due to the Cu dependence of the cytosolic ferro-oxidase enzyme FET3 (53). Bird *et al.* (54) reported that Fe and Cu act synergistically to delay the growth of *Rhodopseudomonas palustris* TIE-1 under anaerobic conditions. It was speculated that Fe(II) might target one or more of the Cu homeostatic system components *cueO*, *copA*, and *cusCFBA*, but the mechanism was unknown (54). Moore *et al.* (55) showed that in *B. subtilis*, a high concentration of Zn led to down-regulation of the CueR regulon by transcriptome profiling and proposed that Zn may act as a weak effector of CueR. Our present study delineated a molecular mechanism underly-

ing the interplay of Zn and Cu homeostatic systems, which is mediated by an intracellular accumulation of Fe. It will be interesting to test whether this metal homeostasis network represents a conserved adaptation mechanism in response to Zn excess in other bacterial species.

Efflux has been demonstrated as an important means of metal detoxification (56). In recent decades, efflux pumps have been increasingly recognized to contribute to the physiology and stress adaptation processes in bacteria. Previously, our group has demonstrated that the CusCFBA efflux pump is induced during anaerobic amino acid limitation to protect [Fe-S] cluster–containing enzymes and its biogenesis in *E. coli* (28). Here we found that the CusCFBA efflux pump is induced during Zn excess to lower the Cu quota in *E. coli* cells and adapt the cells to the stressed condition. Although it is not known currently how dysregulation of the Cue system, which primarily responds to cytosolic Cu, leads to the activation of the Cus system, which responds to periplasmic Cu, the fact that the CusCFBA efflux system is overproduced in these stress adaptation processes and cause Ag tolerance suggests that the phenomenon of cross-resistance is widespread. This phenomenon should not be ignored when the combined metal-based antimicrobials are developed.

Experimental procedures

Bacterial strains and growth conditions

Bacterial strains used in this study are listed in Table S1. *E. coli* cells were cultured in lysogeny broth (LB) for plasmid propagation, strain construction, and FRET assay or in MOPS minimum medium supplemented with 1.32 mM K_2HPO_4 and 0.1% glucose (57) for growth curve, expression, and other analysis. 0.1 mM $ZnSO_4$ was usually added into the MOPS medium to generate Zn stress. When necessary, higher concentrations were added as specified. Antibiotics used in the medium were 20 μg ml^{-1} kanamycin, 25 μg ml^{-1} chloramphenicol, or 10 μg ml^{-1} tetracycline.

Growth curve measurement

Freshly streaked single colonies of tested strains were inoculated into MOPS minimum medium supplemented with 1.32 mM K_2HPO_4 and 0.1% glucose and grown overnight at 37 °C with 220-rpm agitation. Approximately 1×10^6 cells from overnight culture were inoculated into the fresh growth medium indicated and subjected to growth under specified conditions. Cell density was measured based on OD_{600} every 1 h using a spectrophotometer (U-2800, Hitachi), and growth curves were plotted. The results are presented as the mean of three independent isolates.

Construction of single-gene deletion mutant by P1 vir transduction

To prepare the lysate of the donor strain (Keio collection) (58), the Keio collection strain containing the desired mutation was grown in 4 ml of LB medium until OD_{600} reached 0.1–0.2. 100 μl of P1 *vir* and 40 μl of $CaCl_2$ (1 M) was then added into the culture. The mixture was shaken at 37 °C until cells were lysed. Chloroform was added to diminish cell viability. After vortex and centrifugation, supernatant was transferred to a fresh tube and stored at 4 °C. To construct P1 *vir* transduction, the recipient strain was grown in LB medium until OD_{600} exceeded 0.7. After adding 40 μl of $CaCl_2$ (1 M), the culture was shaken for an extra 15 min. 200 μl of recipient cell culture mixed with 100 μl of lysate of the donor strain was incubated at 37 °C for 20 min. 100 μl of citrate (1 M) was added to stop the infection, followed by mixing with 600 μl of LB medium. Mixture was incubated for 1 h and spread on an LB agar plate containing kanamycin and 4 mM citrate. Desirable colonies were screened by colony PCR and DNA sequencing.

Construction of $P_{promoter}$-lacZ transcription reporter (P_{cueO}-lacZ as an example) in the single-copy plasmid pNN387

A DNA fragment corresponding to the bp −164 to −1 region relative to the ATG start codon of *cueO* was amplified using *E. coli* MG1655 genomic DNA as the template and primers specific to this fragment flanked with NotI and HindIII restriction sites at the 5′- and 3′-end, respectively. After digestion with NotI and HindIII, the purified fragment was inserted into the plasmid pNN387, which was treated with the same restriction enzymes (59). After verification by DNA sequencing, plasmid was transformed into AY0416 (MG1655 Δ*lacZ*) for β-gal activity assays (60). Expression of the *lacZ* gene on the plasmid is driven by the *cueO* promoter.

β-Gal activity assay

A β-gal activity assay to measure the *in vivo* transcription of promoter-*lacZ* fusion was performed based on a previous description (61). Cells were grown under specified conditions until OD_{600} reached 0.4. 10 μg ml^{-1} tetracycline was added to stop cell growth and protein synthesis, and cells were left on ice until assayed. 200 μl of cell culture and 800 μl of Z buffer (60 mM Na_2HPO_4, 40 mM NaH_2PO_4, 10 mM KCl, 1 mM $MgCl_2$, 50 mM β-mercaptoethanol, pH 7.0, 4 °C) were mixed. Two drops of chloroform and one drop of 0.1% SDS were added to lyse the cells. The reactions were initiated by adding 200 μl of 4 mg ml^{-1} *ortho*-nitrophenyl-β-galactoside into cell suspension and incubated at 28 °C. Finally, Na_2CO_3 was added to stop the reaction. The expression value in Miller units was calculated, and the results are presented as the mean of three independent isolates.

RT-qPCR

RT-qPCR was performed as described previously (62, 63). Primers for each of the genes tested are listed in Table S2. 4 ml of cells grown under the same conditions as in the β-gal activity assay was subjected to RNA extraction when the OD_{600} reached 0.4. Cells were first mixed with 0.5 ml of ice-cold ethanol/phenol stop solution and placed on ice for 10 min before being harvested by centrifugation at 4,500 rpm for 10 min at 4 °C. After removing the supernatant, the cell pellet was stored at −80 °C to aid cell lysis. Total RNA was extracted using the RNeasy Mini Kit (Qiagen) according to the manufacturer's instructions. Reverse transcription was performed using SuperScript™ II reverse transcriptase (Invitrogen) and random hexamer primers (Invitrogen). qPCR was performed using specific primers mixed with the SYBR Green PCR master mix (Applied

Biosystems) in a 20-μl reaction system. The reaction was performed in an ABI StepOnePlus real-time PCR system. The *E. coli rrsA* gene was utilized as the reference gene to normalize the relative expression of the target genes. The results are expressed as -fold changes of the expression of target genes and presented as the mean of three independent biological isolates.

Western blotting

Bacterial cultures were grown to OD_{600} of 0.4 as described above. Approximately 2.4×10^9 cells were harvested and lysed using the BugBuster protein extraction reagent (Novagen). Supernatant containing the solubilized proteins was mixed with SDS sample buffer (40% glycerol, 8% SDS, 240 mM Tris-HCl, pH 6.8, 0.04% bromphenol blue) and incubated at 55 °C for 25 min. Proteins were separated by SDS-PAGE by using a 10% Tris-glycine polyacrylamide gel and transferred to nitrocellulose membranes by electroblotting. Membranes were subsequently blocked using 5% nonfat milk in TBS-Tween 20 (TBST) followed by immunoblotting using polyclonal anti-FLAG antibody (Sigma-Aldrich) and horseradish peroxidase-conjugated goat anti-rabbit antibody (Sigma-Aldrich). Protein detection was performed using ECL Plus detection reagents (GE Healthcare) to develop the film.

ICP-MS measurements of metal contents

The concentrations of transition metals were measured by ICP-MS on an Agilent 7700x system. Bacterial cells grown in the presence or absence of 0.1 mM Zn were collected at OD_{600} of 0.4 and washed with cold PBS buffer five times. All samples were adjusted to the cell number of 5×10^9 based on their OD_{600} values. After washing, bacterial pellets were subjected to 100 μl of 50% HNO_3 (Fluka) for overnight at 65 °C and then adjusted to a final volume of 1 ml with 1% HNO_3. The standard curves were prepared from multi-element standard solution (Sigma-Aldrich) with six concentrations (*i.e.* 0, 1, 5, 10, 50, 100 ppb) of detected metals. Samples were further diluted when the measured signals exceed the liner range of standard curve. Metal concentrations in the samples were calculated according to the standard curves. For each sample, three biological replicates were performed.

Measurement of intracellular Cu(I) and Fe(II) levels using Cu(I)- and Fe(II)-specific probes

Bacterial cells were grown to OD_{600} of 0.4 in the presence or absence of Zn as described above. Bacterial cells were collected and washed three times with HEPES (for Cu(I)) or PBS (for Fe(II)) buffers, and then 5 μM N4HMF (for Cu(I) analysis) or 10 μM HMRhoNox-M (For Fe(II) analysis) was added. After incubation for 1 h, fluorescence intensity of N4HMF was measured using 485-nm excitation and 528-nm emission and 550-nm excitation and 575-nm emission for the HMRhoNox-M.

Construction of CueR overexpression plasmid and His_6-CueR purification

DNA fragment flanked by the BamHI and NotI sites corresponding to the coding region of *cueR* was amplified using *E. coli* MG1655 genomic DNA as the template. Purified DNA fragment and the pET28a vector were digested with BamHI and NotI. After ligation and DNA sequencing verification, the resulting plasmid was transformed into BL21 for protein expression. Purification of His_6-CueR protein was following the method described previously using the nickel-nitrilotriacetic acid column (Qiagen) (64).

EMSA

To conduct EMSA, DNA fragments of the *copA* and *cueO* promoter regions were first amplified and purified. DNA fragments, CueR protein, and the metal $ZnSO_4$, $CuSO_4$, or $(NH_4)5(Fe(C_6H_4O_7)_2)$ (0.2 mM) were mixed and incubated at 37 °C for 20 min in EMSA binding buffer (100 mM Tris-HCl, pH 8.0, 250 mM NaCl, 25% glycerol). The reaction mixture was subjected to 8% native PAGE at 120 V for 90 min. Free DNA fragment and DNA-protein complex were visualized under UV light after ethidium bromide stain.

Expression of CouA-incorporated CueR and FRET assay

Overnight culture of *E. coli* BL21 (DE3) strain containing the plasmids pET28a-CueR-F58TAG and PEvol-CouRS (38) was diluted 1:100 and grown in LB medium supplemented with kanamycin (20 $\mu g\ ml^{-1}$) and chloramphenicol (25 $\mu g\ ml^{-1}$) to OD_{600} of 0.4. Arabinose (0.04%), isopropyl 1-thio-β-D-galactopyranoside (0.5 mM), and CouA (1 mM) were added subsequently to moderately induce the expression of CouA-labeled CueR. Inducing or interference molecules, such as $CuSO_4$ (0.1 mM), $ZnSO_4$ (0.1 mM), or DIP (0.2 mM), were also added, respectively. After the culture was further incubated for 4.5 h, 6×10^9 cells were harvested and washed once with PBS buffer. Cells were resuspended in 600 μl of PBS. 100 μl of cell suspension was mixed with 15 μl of SYTO9 (50 μM; Invitrogen) and incubated at room temperature in a 96-well black polystyrene plate (Corning) for 15 min. Emission spectra (400–550 nm) of the CouA-SYTO9 FRET complex were recorded with excitation at 360 nm using Thermo Scientific Varioskan® Flash (Thermo Fisher Scientific). FRET efficiency was calculated with the equation, $E = R_0^6/(r^6 + R_0^6)$ (where E is the efficiency of energy transfer; R_0 is the Förster distance, which is the distance between the acceptor and donor when the energy transfer efficiency is 50%; and r is the distance between the acceptor and donor) (65).

Ag and Cu susceptibility assay

Bacterial cells were grown to OD_{600} of 0.4 in the presence or absence of 0.1 mM Zn as described above. Bacterial cells were collected and washed three times with PBS. For the growth-based Ag and Cu susceptibility assay, cell pellets were resuspended to a final cell density of OD_{600} as 0.15 in MOPS medium supplemented with $AgNO_3$ or $CuSO_4$ at the concentrations indicated in Fig. 3*A*. Increased OD (ΔOD) was recorded after cell suspensions were incubated at 37 °C with 220-rpm agitation for 2 h. For the spotting assay, cell pellets were resuspended in MOPS medium supplemented with $CuSO_4$ (final concentration of 4 mM for MG1655 and 3 mM for UTI-1) with a final cell density of OD_{600} of 1.0. Cell suspensions were incubated at 37 °C with 220-rpm agitation for 1 h. Cell suspensions were then serially diluted and spotted on the LB agar plates. The plates were incubated at 37 °C for 16 h.

Competition assay

E. coli MG1655 WT strain and Δ*cusC*::Kn^R strain were used in this assay. Both strains were cultured in MOPS medium and grew overnight at 37 °C with 220-rpm agitation. Overnight cultures of both strains were co-cultured in a ratio of 1:1 in MOPS medium or MOPS medium supplemented with 0.5 mM $ZnSO_4$ until OD_{600} of 0.4. Cell cultures were serially diluted and plated on LB agar plates (for recovery of total cell number) and LB supplemented with kanamycin (20 μg ml^{-1}) (for recovery of Δ*cusC*::Kn^R cells), respectively. The plates were incubated at 37 °C for 16 h. The number of viable *E. coli* cells in the original culture was then calculated from their corresponding cfu. The competitive index is defined as the number of viable Δ*cusC*::Kn^R cells divided by the number of viable WT *E. coli* cells.

Tdh activity assay

Tdh activity was assayed following the methods described previously (21, 66) with slight modifications. Bacterial cells were first grown to OD_{600} of 0.3 as described above. $ZnSO_4$ (final concentration as 0.1 mM) was then added to the cell cultures, and cells were harvested at different time points (5, 15, 30, 60, 120, and 300 min) for the Tdh activity assay. Cells were lysed using the BugBuster protein extraction reagent (Novagen). The assay reaction (200 μl) consisted of 50 mM Tris-HCl buffer (pH 8.4), 1 mM NAD^+, 30 mM L-threonine, and 20 μl of cell lysate and was incubated at 25 °C for 30 min. Production of NADH was measured by the increase of absorbance at 340 nm using the Synergy HTX Plate Reader (BioTek).

Author contributions—Z. X. and A. Y. conceptualization; Z. X. and A. Y. data curation; Z. X. and A. Y. formal analysis; Z. X. visualization; Z. X., P. W., H. W., Z. H. Y., H. Y. A.-Y., T. H., and H. S. methodology; Z. X. writing-original draft; Z. X. and A. Y. writing-review and editing; A. Y. resources; A. Y. supervision; A. Y. funding acquisition; A. Y. validation; A. Y. investigation; A. Y. project administration.

Acknowledgments—We thank Dr. Danny Ka Chun Fung (currently at the Department of Bacteriology, University of Wisconsin, Madison, WI) for constructing E. coli strain expressing chromosomally encoded CusC-FLAG protein. We thank Prof. Patrick C. Y. Woo (Department of Microbiology, University of Hong Kong) for providing the clinically isolated uropathogenic E. coli strain.

References

1. Andreini, C., Bertini, I., Cavallaro, G., Holliday, G. L., and Thornton, J. M. (2008) Metal ions in biological catalysis: from enzyme databases to general principles. *J. Biol. Inorg. Chem.* **13,** 1205–1218 CrossRef Medline
2. Dudev, T., and Lim, C. (2014) Competition among metal ions for protein binding sites: determinants of metal ion selectivity in proteins. *Chem. Rev.* **114,** 538–556 CrossRef Medline
3. Macomber, L., and Imlay, J. A. (2009) The iron-sulfur clusters of dehydratases are primary intracellular targets of copper toxicity. *Proc. Natl. Acad. Sci. U.S.A.* **106,** 8344–8349 CrossRef Medline
4. Jomova, K., and Valko, M. (2011) Advances in metal-induced oxidative stress and human disease. *Toxicology* **283,** 65–87 CrossRef Medline
5. Xu, F. F., and Imlay, J. A. (2012) Silver(I), mercury(II), cadmium(II), and zinc(II) target exposed enzymic iron-sulfur clusters when they toxify *Escherichia coli*. *Appl. Environ. Microbiol.* **78,** 3614–3621 CrossRef Medline
6. Braymer, J. J., and Giedroc, D. P. (2014) Recent developments in copper and zinc homeostasis in bacterial pathogens. *Curr. Opin. Chem. Biol.* **19,** 59–66 CrossRef Medline
7. Hood, M. I., and Skaar, E. P. (2012) Nutritional immunity: transition metals at the pathogen-host interface. *Nat. Rev. Microbiol.* **10,** 525–537 CrossRef Medline
8. Djoko, K. Y., Ong, C. L., Walker, M. J., and McEwan, A. G. (2015) The role of copper and zinc toxicity in innate immune defense against bacterial pathogens. *J. Biol. Chem.* **290,** 18954–18961 CrossRef Medline
9. Schaible, U. E., Collins, H. L., Priem, F., and Kaufmann, S. H. E. (2002) Correction of the iron overload defect in β-2-microglobulin knockout mice by lactoferrin abolishes their increased susceptibility to tuberculosis. *J. Exp. Med.* **196,** 1507–1513 CrossRef Medline
10. Chandrangsu, P., Rensing, C., and Helmann, J. D. (2017) Metal homeostasis and resistance in bacteria. *Nat. Rev. Microbiol.* **15,** 338–350 CrossRef Medline
11. White, C., Lee, J., Kambe, T., Fritsche, K., and Petris, M. J. (2009) A role for the ATP7A copper-transporting ATPase in macrophage bactericidal activity. *J. Biol. Chem.* **284,** 33949–33956 CrossRef Medline
12. Wolschendorf, F., Ackart, D., Shrestha, T. B., Hascall-Dove, L., Nolan, S., Lamichhane, G., Wang, Y., Bossmann, S. H., Basaraba, R. J., and Niederweis, M. (2011) Copper resistance is essential for virulence of *Mycobacterium tuberculosis*. *Proc. Natl. Acad. Sci. U.S.A.* **108,** 1621–1626 CrossRef Medline
13. Jacobsen, F. E., Kazmierczak, K. M., Lisher, J. P., Winkler, M. E., and Giedroc, D. P. (2011) Interplay between manganese and zinc homeostasis in the human pathogen *Streptococcus pneumoniae*. *Metallomics* **3,** 38–41 CrossRef Medline
14. Wagner, D., Maser, J., Lai, B., Cai, Z., Barry, C. E., 3rd, Höner Zu Bentrup, K., Russell, D. G., and Bermudez, L. E. (2005) Elemental analysis of *Mycobacterium avium*-, *Mycobacterium tuberculosis*-, and *Mycobacterium smegmatis*-containing phagosomes indicates pathogen-induced microenvironments within the host cell's endosomal system. *J. Immunol.* **174,** 1491–1500 CrossRef Medline
15. Corbin, B. D., Seeley, E. H., Raab, A., Feldmann, J., Miller, M. R., Torres, V. J., Anderson, K. L., Dattilo, B. M., Dunman, P. M., Gerads, R., Caprioli, R. M., Nacken, W., Chazin, W. J., and Skaar, E. P. (2008) Metal chelation and inhibition of bacterial growth in tissue abscesses. *Science* **319,** 962–965 CrossRef Medline
16. Liu, J. Z., Jellbauer, S., Poe, A. J., Ton, V., Pesciaroli, M., Kehl-Fie, T. E., Restrepo, N. A., Hosking, M. P., Edwards, R. A., Battistoni, A., Pasquali, P., Lane, T. E., Chazin, W. J., Vogl, T., Roth, J., *et al.* (2012) Zinc sequestration by the neutrophil protein calprotectin enhances *Salmonella* growth in the inflamed gut. *Cell Host Microbe* **11,** 227–239 CrossRef Medline
17. Botella, H., Peyron, P., Levillain, F., Poincloux, R., Poquet, Y., Brandli, I., Wang, C., Tailleux, L., Tilleul, S., Charrière, G. M., Waddell, S. J., Foti, M., Lugo-Villarino, G., Gao, Q., Maridonneau-Parini, I., *et al.* (2011) Mycobacterial P1-type ATPases mediate resistance to zinc poisoning in human macrophages. *Cell Host Microbe* **10,** 248–259 CrossRef Medline
18. Porcheron, G., Garénaux, A., Proulx, J., Sabri, M., and Dozois, C. M. (2013) Iron, copper, zinc, and manganese transport and regulation in pathogenic Enterobacteria: correlations between strains, site of infection and the relative importance of the different metal transport systems for virulence. *Front. Cell Infect. Microbiol.* **3,** 90 CrossRef Medline
19. McDevitt, C. A., Ogunniyi, A. D., Valkov, E., Lawrence, M. C., Kobe, B., McEwan, A. G., and Paton, J. C. (2011) A molecular mechanism for bacterial susceptibility to zinc. *PLoS Pathog.* **7,** e1002357 CrossRef Medline
20. Chandrangsu, P., and Helmann, J. D. (2016) Intracellular Zn(II) intoxication leads to dysregulation of the perr regulon resulting in heme toxicity in *Bacillus subtilis*. *PLoS Genet.* **12,** e1006515 CrossRef Medline
21. Gu, M., and Imlay, J. A. (2013) Superoxide poisons mononuclear iron enzymes by causing mismetallation. *Mol. Microbiol.* **89,** 123–134 CrossRef Medline
22. Kapetanovic, R., Bokil, N. J., Achard, M. E., Ong, C.-L. Y., Peters, K. M., Stocks, C. J., Phan, M.-D., Monteleone, M., Schroder, K., and Irvine, K. M., Saunders, B. M., Walker, M. J., Stacey, K. J., McEwan, A. G., Schembri,

M. A., and Sweet, M. J. (2016) *Salmonella* employs multiple mechanisms to subvert the TLR-inducible zinc-mediated antimicrobial response of human macrophages. *FASEB J.* **30,** 1901–1912 CrossRef Medline
23. Ong, C.-L. Y., Walker M. J., and McEwan, A. G. (2015) Zinc disrupts central carbon metabolism and capsule biosynthesis in *Streptococcus pyogenes*. *Sci Rep.* **5,** 10799 CrossRef Medline
24. Hassan, K. A., Pederick, V. G., Elbourne, L. D., Paulsen, I. T., Paton, J. C., McDevitt, C. A., and Eijkelkamp, B. A. (2017) Zinc stress induces copper depletion in *Acinetobacter baumannii*. *BMC Microbiol.* **17,** 59 CrossRef Medline
25. Taki, M., Iyoshi, S., Ojida, A., Hamachi, I., and Yamamoto, Y. (2010) Development of highly sensitive fluorescent probes for detection of intracellular copper (I) in living systems. *J. Am. Chem. Soc.* **132,** 5938–5939 CrossRef Medline
26. Tsugawa, H., Mori, H., Matsuzaki, J., Masaoka, T., Hirayama, T., Nagasawa, H., Sakakibara, Y., Suematsu, M., and Suzuki, H. (2015) Nordihydroguaiaretic acid disrupts the antioxidant ability of *Helicobacter pylori* through the repression of SodB activity *in vitro*. *Biomed. Res. Int.* **2015,** 734548 CrossRef Medline
27. Lee, L. J., Barrett, J. A., and Poole, R. K. (2005) Genome-wide transcriptional response of chemostat-cultured *Escherichia coli* to zinc. *J. Bacteriol.* **187,** 1124–1134 CrossRef Medline
28. Fung, D. K., Lau, W. Y., Chan, W. T., and Yan, A. (2013) Copper efflux is induced during anaerobic amino acid limitation in *Escherichia coli* to protect iron-sulfur cluster enzymes and biogenesis. *J. Bacteriol.* **195,** 4556–4568 CrossRef Medline
29. Gudipaty, S. A., Larsen, A. S., Rensing, C., and McEvoy, M. M. (2012) Regulation of Cu(I)/Ag(I) efflux genes in *Escherichia coli* by the sensor kinase CusS. *FEMS Microbiol. Lett.* **330,** 30–37 CrossRef Medline
30. Munson, G. P., Lam, D. L., Outten, F. W., and O'Halloran, T. V. (2000) Identification of a copper-responsive two-component system on the chromosome of *Escherichia coli* K-12. *J. Bacteriol.* **182,** 5864–5871 CrossRef Medline
31. Harmon, H. J., and Crane, F. L. (1974) Inhibition of cytochrome *c* oxidase by hydrophobic metal chelators. *Biochim. Biophys. Acta* **368,** 125–129 CrossRef Medline
32. Outten, F. W., Outten, C. E., Hale, J., and O'Halloran, T. V. (2000) Transcriptional activation of an *Escherichia coli* copper efflux regulon by the chromosomal MerR homologue, CueR. *J. Biol. Chem.* **275,** 31024–31029 CrossRef Medline
33. Outten, F. W., Huffman, D. L., Hale, J. A., and O'Halloran, T. V. (2001) The independent *cue* and *cus* systems confer copper tolerance during aerobic and anaerobic growth in *Escherichia coli*. *J. Biol. Chem.* **276,** 30670–30677 CrossRef Medline
34. Rensing, C., Fan, B., Sharma, R., Mitra, B., and Rosen, B. P. (2000) CopA: an *Escherichia coli* Cu(I)-translocating P-type ATPase. *Proc. Natl. Acad. Sci. U.S.A.* **97,** 652–656 CrossRef Medline
35. Osman, D., and Cavet, J. S. (2008) Copper homeostasis in bacteria. *Adv. Appl. Microbiol.* **65,** 217–247 CrossRef Medline
36. Grass, G., and Rensing, C. (2001) CueO is a multi-copper oxidase that confers copper tolerance in *Escherichia coli*. *Biochem. Biophys. Res. Commun.* **286,** 902–908 CrossRef Medline
37. Philips, S. J., Canalizo-Hernandez, M., Yildirim, I., Schatz, G. C., Mondragón, A., and O'Halloran, T. V. (2015) Allosteric transcriptional regulation via changes in the overall topology of the core promoter. *Science* **349,** 877–881 CrossRef Medline
38. Wang, J., Xie, J., and Schultz, P. G. (2006) A genetically encoded fluorescent amino acid. *J. Am. Chem. Soc.* **128,** 8738–8739 CrossRef Medline
39. Postle, K. (1990) Aerobic regulation of the *Escherichia coli tonB* gene by changes in iron availability and the *fur* locus. *J. Bacteriol.* **172,** 2287–2293 CrossRef Medline
40. Touati, D. (2000) Iron and oxidative stress in bacteria. *Arch. Biochem. Biophys.* **373,** 1–6 CrossRef Medline
41. Kristiansen, K. A., Jensen, P. E., Møller, I. M., and Schulz, A. (2009) Monitoring reactive oxygen species formation and localisation in living cells by use of the fluorescent probe CM-H_2DCFDA and confocal laser microscopy. *Physiol. Plant* **136,** 369–383 CrossRef Medline
42. Lai, Y., Xu, Z., and Yan, A. (2017) A novel regulatory circuit to control indole biosynthesis protects *Escherichia coli* from nitrosative damages during the anaerobic respiration of nitrate. *Environ. Microbiol.* **19,** 598–610 CrossRef Medline
43. Botella, H., Stadthagen, G., Lugo-Villarino, G., de Chastellier, C., and Neyrolles, O. (2012) Metallobiology of host-pathogen interactions: an intoxicating new insight. *Trends Microbiol.* **20,** 106–112 CrossRef Medline
44. Neyrolles, O., Wolschendorf, F., Mitra, A., and Niederweis, M. (2015) Mycobacteria, metals, and the macrophage. *Immunol. Rev.* **264,** 249–263 CrossRef Medline
45. Irving, H., and Williams, R. (1948) Order of stability of metal complexes. *Nature* **162,** 746–747 CrossRef
46. Imlay, J. A. (2014) The mismetallation of enzymes during oxidative stress. *J. Biol. Chem.* **289,** 28121–28128 CrossRef Medline
47. Osman, D., Martini, M. A., Foster, A. W., Chen, J., Scott, A. J. P., Morton, R. J., Steed, J. W., Lurie-Luke, E., Huggins, T. G., Lawrence, A. D., Deery, E., Warren, M. J., Chivers, P. T., and Robinson, N. J. (2019) Bacterial sensors define intracellular free energies for correct enzyme metalation. *Nat. Chem. Biol.* **15,** 241–249 CrossRef Medline
48. Osman, D., Foster, A. W., Chen, J., Svedaite, K., Steed, J. W., Lurie-Luke, E., Huggins, T. G., and Robinson, N. J. (2017) Fine control of metal concentrations is necessary for cells to discern zinc from cobalt. *Nat. Commun.* **8,** 1884 CrossRef Medline
49. Mills, S. A., and Marletta, M. A. (2005) Metal binding characteristics and role of iron oxidation in the ferric uptake regulator from *Escherichia coli*. *Biochemistry* **44,** 13553–13559 CrossRef Medline
50. Foster, A. W., Osman, D., and Robinson, N. J. (2014) Metal preferences and metallation. *J. Biol. Chem.* **289,** 28095–28103 CrossRef Medline
51. Outten, C. E., and O'Halloran, T. V. (2001) Femtomolar sensitivity of metalloregulatory proteins controlling zinc homeostasis. *Science* **292,** 2488–2492 CrossRef Medline
52. Graham, A. I., Sanguinetti, G., Bramall, N., McLeod, C. W., and Poole, R. K. (2012) Dynamics of a starvation-to-surfeit shift: a transcriptomic and modelling analysis of the bacterial response to zinc reveals transient behaviour of the Fur and SoxS regulators. *Microbiology* **158,** 284–292 CrossRef Medline
53. Dancis, A., Yuan, D. S., Haile, D., Askwith, C., Eide, D., Moehle, C., Kaplan, J., and Klausner, R. D. (1994) Molecular characterization of a copper transport protein in *S. cerevisiae*: an unexpected role for copper in iron transport. *Cell* **76,** 393–402 CrossRef Medline
54. Bird, L. J., Coleman, M. L., and Newman, D. K. (2013) Iron and copper act synergistically to delay anaerobic growth of bacteria. *Appl. Environ. Microbiol.* **79,** 3619–3627 CrossRef Medline
55. Moore, C. M., Gaballa, A., Hui, M., Ye, R. W., and Helmann, J. D. (2005) Genetic and physiological responses of *Bacillus subtilis* to metal ion stress. *Mol. Microbiol.* **57,** 27–40 CrossRef Medline
56. Xu, Z., and Yan, A. (2015) Multidrug efflux systems in microaerobic and anaerobic bacteria. *Antibiotics* **4,** 379–396 CrossRef Medline
57. Neidhardt, F. C., Bloch, P. L., and Smith, D. F. (1974) Culture medium for enterobacteria. *J. Bacteriol.* **119,** 736–747 Medline
58. Baba, T., Ara, T., Hasegawa, M., Takai, Y., Okumura, Y., Baba, M., Datsenko, K. A., Tomita, M., Wanner, B. L., and Mori, H. (2006) Construction of *Escherichia coli* K-12 in-frame, single-gene knockout mutants: the Keio collection. *Mol. Syst. Biol.* **2,** 2006.0008 CrossRef Medline
59. Elledge, S. J., and Davis, R. W. (1989) Position and density effects on repression by stationary and mobile DNA-binding proteins. *Genes Dev.* **3,** 185–197 CrossRef Medline
60. Zhang, Y., Xiao, M., Horiyama, T., Zhang, Y., Li, X., Nishino, K., and Yan, A. (2011) The multidrug efflux pump MdtEF protects against nitrosative damage during the anaerobic respiration in *Escherichia coli*. *J. Biol. Chem.* **286,** 26576–26584 CrossRef Medline
61. Deng, Z., Shan, Y., Pan, Q., Gao, X., and Yan, A. (2013) Anaerobic expression of the *gadE-mdtEF* multidrug efflux operon is primarily regulated by the two-component system ArcBA through antagonizing the H-NS mediated repression. *Front. Microbiol.* **4,** 194 CrossRef Medline
62. Bustin, S. A., Benes, V., Garson, J. A., Hellemans, J., Huggett, J., Kubista, M., Mueller, R., Nolan, T., Pfaffl, M. W., Shipley, G. L., Vandesompele, J., and Wittwer, C. T. (2009) The MIQE guidelines: minimum information

for publication of quantitative real-time PCR experiments. *Clin. Chem.* **55,** 611–622 CrossRef Medline

63. Schmittgen, T. D., and Livak, K. J. (2008) Analyzing real-time PCR data by the comparative C_T method. *Nat. Protoc.* **3,** 1101–1108 CrossRef Medline
64. Bekker, M., Alexeeva, S., Laan, W., Sawers, G., Teixeira de Mattos, J., and Hellingwerf, K. (2010) The ArcBA two-component system of *Escherichia coli* is regulated by the redox state of both the ubiquinone and the menaquinone pool. *J. Bacteriol.* **192,** 746–754 CrossRef Medline
65. Stryer, L. (1978) Fluorescence energy transfer as a spectroscopic ruler. *Annu. Rev. Biochem.* **47,** 819–846 CrossRef Medline
66. Boylan, S. A., and Dekker, E. E. (1981) L-threonine dehydrogenase: purification and properties of the homogeneous enzyme from *Escherichia coli* K-12. *J. Biol. Chem.* **256,** 1809–1815 Medline